AIAA-93-3331-CP

NUMERICAL WAVE PROPAGATION AND STEADY STATE SOLUTIONS: (II) BULK VISCOSITY DAMPING

K. Mazaheri* and P. L. Roe† The University of Michigan, Ann Arbor, Michigan

ABSTRACT

Error waves in the computational field may be damped by adding a bulk viscosity term to the momentum equations. We analyse the effects on the linearized differential equations, and study its explicit and implicit implementations in one space dimension. Optimum values of the Bulk Viscosity Damping (BVD) coefficients are discussed. After generalizing the idea to two space dimensions, its performance both alone and in combination with a soft wall boundary condition and residual smoothing in central differencing codes is reviewed. It is shown that BVD is complementary to residual smoothing, and acts independently of it. It is also shown how this new term can stabilize and accelerate the computation of low Mach number flows.

1 INTRODUCTION

An effective strategy to accelerate convergence of Euler solvers, is to damp the residual waves while they are traversing the flow field. There are several ways to do this, like multigrid and residual smoothing. Here one systematic and very simple way is developed to do this, consistent with the methodology in handling the residual waves presented in [1].

The idea generalizes one recently presented by Ramshaw and Mousseau [2] for accelerating the convergence of incompressible flow calculations. They added an *artificial bulk viscosity* term to a code based on the artificial compressibility method introduced in 1967 by Chorin [3]. Apparently nobody has tried to use this idea in genuinely compressible calculations. To do this, we have to take a slightly non-physical approach, so that the added terms will vanish in the steady state. In this paper we construct an artificial bulk viscosity, which does vanish when required, and can be tuned to damp out the error waves. The motivation comes from the fact that the acoustic waves are primarily responsible for the slow convergence. [1]

*Graduate Research Assistant, Aerospace Engineering. Present Address; Sharif University of Technology,Tehran, Iran

†Professor, Aerospace Engineering, Senior Member.

[1] For further details of the material in this paper, see [4]

2 THEORY OF BULK VISCOSITY DAMPING (BVD)

2.1 DEFINITION

The *Navier Stokes'* momentum equation can be written as:

$$\frac{\partial}{\partial t}(\rho \mathbf{u}) + \mathrm{div}(\rho \mathbf{u} : \mathbf{u}) = \rho \mathbf{f} + \nabla \cdot \mathbf{T},$$

where the stress tensor $\mathbf{T}$ includes three terms:

$$\mathbf{T} = -p\ \delta_{ij} + \lambda\ \mathrm{div}(\mathbf{u})\delta_{ij} + 2\mu\epsilon_{ij}. \qquad (1)$$

Here, λ and μ are respectively the bulk viscosity and the shear viscosity coefficients. The bulk viscosity is the part of the viscous stress which is proportional to the divergence of the velocity. For positive λ, bulk viscosity increases the internal energy in proportion to $(\mathrm{div}(\mathbf{u}))^2$ and dissipates the acoustic waves.

For incompressible flow the velocity divergence vanishes in the steady state, and adding an artificial term proportional to its gradient will leave the steady state unchanged. This was the approach taken in [2]. For compressible flow, a similar effect can be achieved using the divergence of $\rho\mathbf{u}$, that is to say, $-\rho_t$.

For computation with the inviscid equations, we will use

$$\mathbf{T} = -(p + a\, l\, \rho_t)\ \delta_{ij}, \qquad (2)$$

where a is the local sound speed and l is an artificial bulk viscosity coefficient with the dimension of length. This constant needs to be determined by design criteria, or stability restrictions (found by analysis, or empirically).

2.2 ONE DIMENSIONAL ACOUSTIC EQUATIONS

To analyse the effect of the new term, *the linearized Euler equations* (i.e. *acoustic equations*) in one space dimension will be considered here. After adding the new term we will have:

$$\begin{aligned} \rho_t + \rho_0 u_x &= 0, \\ u_t + \frac{1}{\rho_0} p_x + \frac{a_0 l}{\rho_0} \rho_{xt} &= 0, \\ p_t + \rho_0 a_0^2 u_x &= 0. \end{aligned} \qquad (3)$$

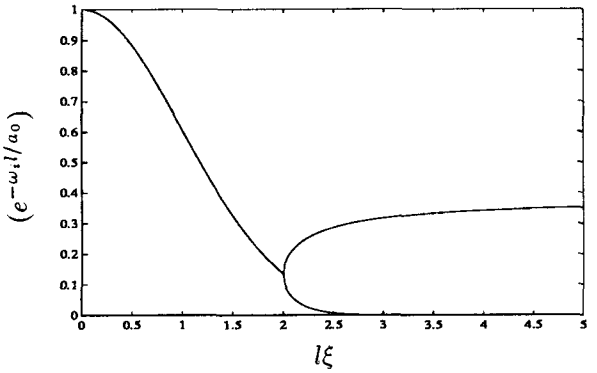

Figure 1: Damping $(e^{-\omega_i l/a_0})$ for different wave numbers $l\xi$

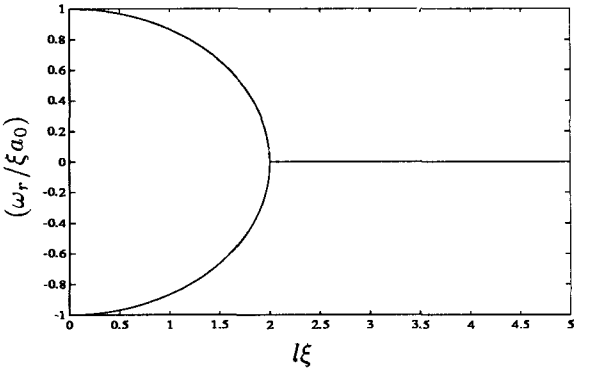

Figure 2: Wave speed $(\omega_r/\xi a_0)$ for different wave numbers $l\xi$

Let's require solutions of the form:

$$\mathbf{u} = \mathcal{R}e(U) \quad \exp\ i(\omega t - \xi x).$$

Here, $\mathcal{I}m(\xi) = 0$, in order to have bounded solutions for large x, but $\omega = \omega_r + i\omega_i$. Substitution of this form of solution in the above equations, and requiring non-trivial solutions, yields the dispersion relation:

$$\det \begin{vmatrix} i\omega & -i\rho_0\xi & 0 \\ \frac{a_0 l}{\rho_0}\omega\xi & i\omega & -\frac{i\xi}{\rho_0} \\ 0 & -i\xi\rho_0 a_0^2 & i\omega \end{vmatrix} = 0,$$

After substituting the real and imaginary parts of ω (if $\omega \neq 0$), and solving the imaginary and real parts of the dispersion equation, one finds two different cases:

- $\omega_r = 0$, and

$$\frac{\omega_i l}{a_0} = (l\xi)^2 \left(\frac{1}{2} \pm \sqrt{\frac{1}{4} - (\frac{1}{l\xi})^2}\right),$$

  which is valid for $(l\xi)^2 \geq 4$.

- $\omega_i = \frac{1}{2}a_0 l\xi^2$, and

$$\frac{\omega_r}{\xi a_0} = \pm\sqrt{1 - \left(\frac{l\xi}{2}\right)^2},$$

  for $(l\xi)^2 < 4$.

The nondimensionalized variation of wavespeeds $\frac{\omega_r l}{a_0}$ and damping $e^{-\omega_i l/a_0}$ for different wavenumbers are plotted in Figures 1 and 2. Figure 1 shows that high frequencies are heavily damped. Figure 2 shows that on the differential level the high frequencies are not allowed to propagate at all, which is in a sense an advantage, since then one won't be worried about their reflections from the boundaries, and moving forward and backward in the flow field. At the same time, the advantage of convecting them out of the flow field is lost.

2.3 Stability Analysis

To see effects of the new term on numerical stability, let's consider the following system of equations:

$$\begin{aligned} u_t + \frac{1}{\rho_0}p_x &= a_0 l u_{xx}, \\ p_t + \rho_0 a_0^2 u_x &= 0. \end{aligned} \tag{4}$$

Analytically, these have the same dispersion relationship (apart from a nonpropagating factor) as (3). One can write the equations in characteristic form:

$$\begin{pmatrix} q \\ r \end{pmatrix}_t + \begin{bmatrix} a_0 & 0 \\ 0 & -a_0 \end{bmatrix} \begin{pmatrix} q \\ r \end{pmatrix}_x = a_0^2 l\rho_0 \begin{pmatrix} u_{xx} \\ -u_{xx} \end{pmatrix},$$

where

$$\begin{pmatrix} q \\ r \end{pmatrix} = \begin{pmatrix} p + \rho_0 a_0 u \\ p - \rho_0 a_0 u \end{pmatrix}.$$

Using upwind differencing on the left hand side, and central differencing on the right hand side, and assuming solutions of the form $\mathbf{u}_j^n = \mathbf{U}_o \exp i(n\Omega + j\beta)$ one finds the discrete amplification matrix in the original variables as

$$\hat{\mathbf{G}} = \begin{bmatrix} 1 + \nu(\cos\beta - 1) + 2\gamma(\cos\beta - 1) & -i\frac{\nu}{a_0\rho_0}\sin\beta \\ -i\nu a_0\rho_0 \sin\beta & 1 + \nu(\cos\beta - 1) \end{bmatrix}.$$

where $\gamma = \nu\frac{l}{\Delta x}$. To have bounded solutions, the spectral radius of $\hat{\mathbf{G}}$ should be equal to or less than one. The eigenvalues of $\hat{\mathbf{G}}$ are roots of the quadratic equation:

$$\lambda^2 - 2\left(1 + (\nu + \gamma)(\cos\beta - 1)\right)\lambda + \nu^2 \sin^2\beta$$
$$+ [1 + \nu(\cos\beta - 1)]\,[1 + (\nu + 2\gamma)(\cos\beta - 1)] = 0.$$

One can show that stability requires

$$\nu + 2\gamma \leq 1.$$

Assuming that ν is determined in advance, one needs

$$\frac{l}{\Delta x} \leq \left(\frac{1 - \nu}{2\nu}\right). \tag{5}$$

Thus, for a simple explicit discretization, the coefficient l cannot be large compared with the mesh size. This is natural, since we have added a parabolic term to the equations. In practice, as will be seen in the next sections, the stability margin on practical stencils is often wider than this estimate suggests. However, we certainly need to keep in mind the possibility of implementing BVD implicitly.

3 Application In One Space Dimension

3.1 Modification of the Euler Equations

ONE SPACE DIMENSION

After modification, the resulting equations are

$$\begin{pmatrix} \rho \\ \rho u \\ \rho E \end{pmatrix}_t + \begin{pmatrix} \rho u \\ \rho u^2 + p \\ \rho u H \end{pmatrix}_x = \begin{pmatrix} 0 \\ -la\rho_{xt} \\ 0 \end{pmatrix}.$$

It would also be possible to add an 'artificial pressure' to the energy equation. However, we have yet to find any benefit from doing this.

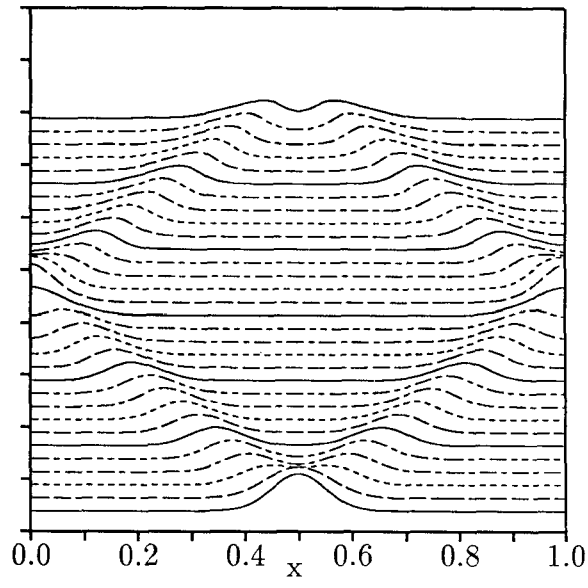

Figure 3: Linear wave evolution by original Euler equations.

3.2 Explicit Numerical Discretization

The numerical method used here is an explicit first-order upwind method. The update procedure for the momentum equation will be slightly changed:

$$(\rho u)_j^{n+1} = (\rho u)_j^n - \frac{\Delta t}{\Delta x}(F^{\star^n}_{2,j+\frac{1}{2}} + F^{\star^n}_{2,j-\frac{1}{2}})$$

$$-l\ a\frac{(\rho_t)^n_{j+1} - (\rho_t)^n_{j-1}}{2\Delta x},$$

where

$$(\rho_t)^n_j = -\ \frac{F^{\star^n}_{1,j+\frac{1}{2}} + F^{\star^n}_{1,j-\frac{1}{2}}}{\Delta x},$$

and $F^{\star^n}_{2,j+\frac{1}{2}}$ is the second element of the flux vector, evaluated at the interface of cells j and $j+1$ at time step n (here computed using the Roe averages, but any good flux formula could be used). This seems to be the simplest way to create a discretization that is conservative, and for which the added terms vanish in the steady state. However, the stencil is effectively extended to five cells by the form of the BVD term. This appears to enlarge the stability margins found in the previous section.

The boundary condition for the extra term is applied using ghost cells, and ρ_t in the ghost cells is chosen to be zero.

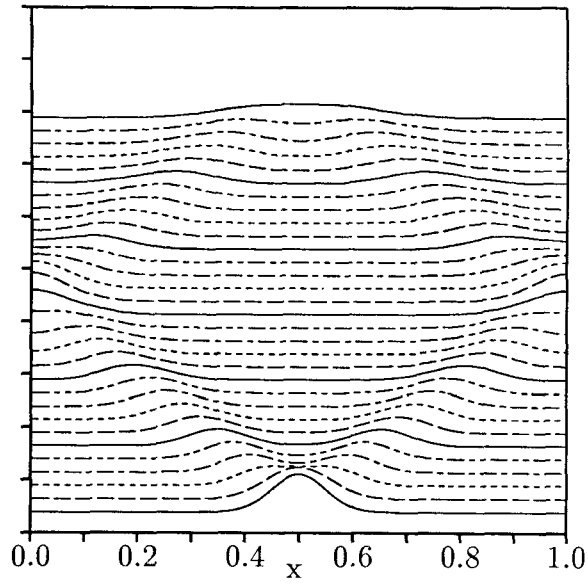

Figure 4: Linear wave evolution by modified Euler equations. Here $l/\Delta x = 0.5$

3.3 Explicit Numerical Computations

To see the effect of the new term on the evolution of the flow field, computations are done in a pressure-tube. Assume $0 < x < 1$ and $t > 0$. Solid walls are assumed at both ends. For the initial condition, the fluid is assumed to be still everywhere, with uniform density ρ_0, and with a Gaussian distribution for pressure:

$$u = 0 \qquad \rho = \rho_0 \qquad p = p_0(1 + \alpha e^{-\beta(x+0.5)^2}),$$

where β is a constant of order 100, and α is a constant equal to 0.1 or 1.0 which determines the strength of the initial pressure disturbance. Choosing $\alpha = 1.0$ will allow non-linear waves be generated, and these will collapse in a very strong shock wave. Using a global time-stepping procedure, Figure 3 shows the wave evolutions for $\alpha = 0.1$, which is weak enough to stay linear, without bulk viscosity. The horizontal axis is the space dimension, $0 < x < 1$; the grid employs 100 cells. The curves shown are pressure distributions at different times; the lowest curve is the initial condition.

The (almost perfect) reflection of the right and left-going waves at the solid wall can be observed. This figure shows that although a first-order dissipative method is used, the waves will bounce back and forth several times, before being dissipated in the flow field. Figure 4 shows how the smooth waves are dissipated fairly effectively in the first period of their movement, after addition of slight bulk viscosity with $l = \frac{\Delta x}{2}$. With this value of l, the regular explicit timestep for the unmodified problem could be used.

To see how everything works at the nonlinear level, a high amplitude initial pressure distribution ($\alpha = 1$) is used. Figure 5 shows that strong shock waves are generated in the absence of bulk viscosity damping. Again, even in our first-order upwind code, shocks will move forward and backward for hundreds of periods of the wave.

Figure 6 shows that addition of small bulk viscosity ($l = \frac{\Delta x}{2}$, again small enough to keep the regular time-steps stable) not only prohibits shock generation, but also dissipates the wave as well before it accomplishes its first round trip. The amount of extra computation in both the linear and nonlinear cases is the same, and in the above mentioned code it's quite negligible ($\approx 1\%$). Larger values of l, although more effective in damping, require a substantial decrease in the time-steps.

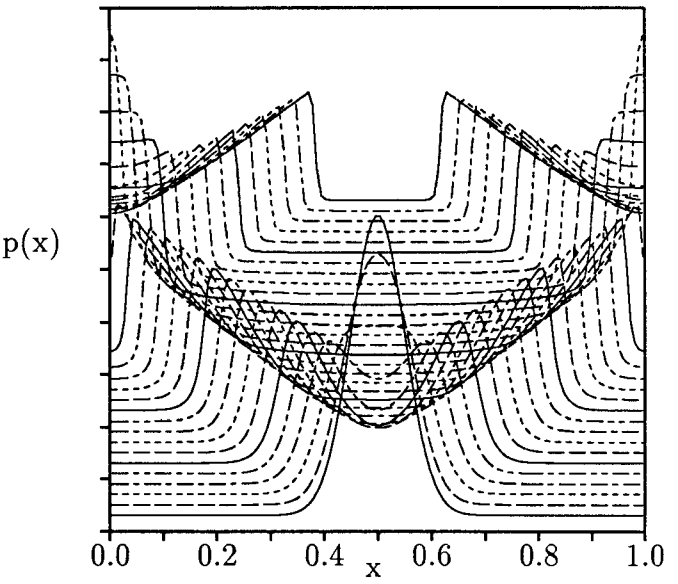

Figure 5: Nonlinear wave evolution by original Euler equations.

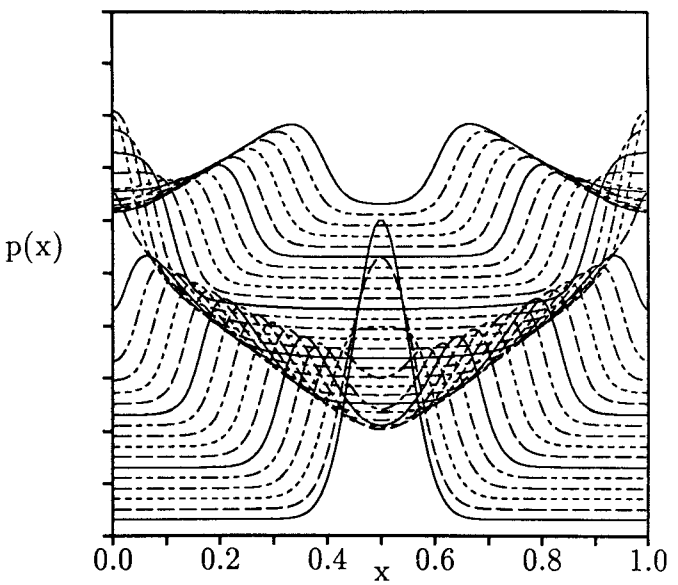

Figure 6: Nonlinear wave evolution by modified Euler equations. Here $l/\Delta x = 0.5$.

3.4 Implicit Numerical Discretization

To cure the stiffness generated by the new term, one needs to introduce some level of implicit evaluation to make high values of damping possible. Since the troublesome term appears only in the momentum equation, only this

equation needs to be treated implicitly. To do so, one needs to substitute ρ_t in the momentum equation with $-(\rho u)_x$. The modified momentum equation is then:

$$(\rho u)_t + (p + \rho u^2)_x - la \ \ (\rho u)_{xx} = 0,$$

and its update formula will be:

$$(\rho u)_j^{n+1} = (\rho u)_j^n - \frac{\Delta t}{\Delta x}(F^{\star^n}_{2,j+\frac{1}{2}} + F^{\star^n}_{2,j-\frac{1}{2}})$$

$$-l\ a\frac{\Delta t}{\Delta x}((\rho u)_{j+1}^{n+1} - 2(\rho u)_j^{n+1} + (\rho u)_{j-1}^{n+1}).$$

The last term (damping term) may not always vanish identically in the steady state. However, some loss of this desirable property seems to be inescapable with any conveniently implemented implicit scheme. In each time step, first $(\rho)^n$ and $(\rho E)^n$ will be explicitly updated as usual, and then the discretized momentum equation will be solved. The momentum equation results in an $N \times N$ tridiagonal system, where the diagonal terms are $(1+2\beta)$, and the off-diagonal terms are $-\beta$, where

$$\beta = \frac{la\Delta t}{\Delta x^2} > 0.$$

Boundary conditions for the new term requires value of ρu at ghost cells, which are trivial for the solid wall BC. For other boundary conditions, one may use the fact that $(\rho u)_{xx} = -(\rho_t)_x$ and

$$\rho_t = \frac{\rho_j^{n+1} - \rho_j^n}{\Delta t},$$

which gives the alternative form

$$(\rho u)_{xx}|_j^{n+1} = -\frac{(\rho_t)_{j+1} + (\rho_t)_{j-1}}{2\Delta x}.$$

The unknowns are $(\rho u)_i^{n+1}$, and the right hand side vector of the system is

$$\begin{pmatrix} \cdots + \beta(\rho u)_0^n \\ \cdots \\ (\rho u)_i^n - \frac{\Delta t}{\Delta x}(F^{\star^n}_{2,i+\frac{1}{2}} + F^{\star^n}_{2,i-\frac{1}{2}}) \\ \cdots \\ \cdots + \beta(\rho u)_{N+1}^n \end{pmatrix}.$$

Note that the system is diagonally dominant, and can be solved efficiently by standard tri-diagonal solvers. The amount of extra work for solving this system is hardly visible.

3.5 Implicit Numerical Computations

Similar experiments to Section 3.3 are done to see by how much it is worth increasing this damping term.

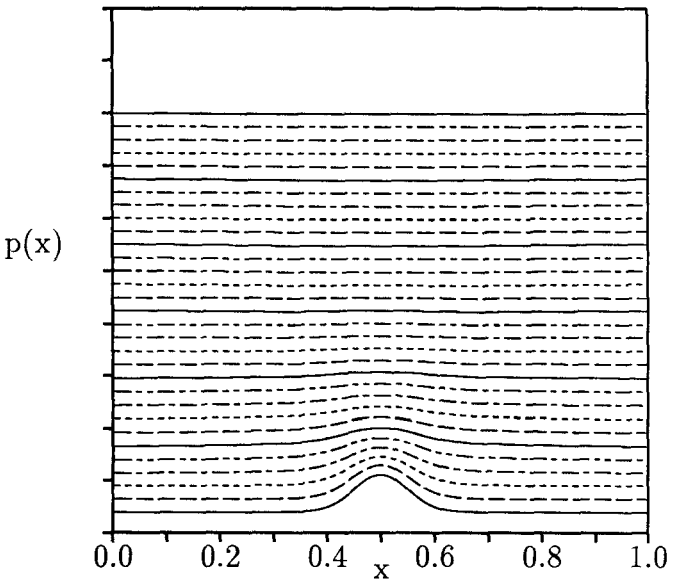

Figure 7: Linear wave evolution by modified Euler equations, $\frac{l}{\Delta x} = 25$

Figure 7 shows the linear wave (i.e. wave with small initial amplitude), with bulk viscosity corresponding to $\frac{l}{\Delta x} = 25$. For this data, the analysis of section 2.2 predicts that any value of l greater than about $6\Delta x$ will result in very little wave propagation, and mostly static dissipation. This is the effect seen in Figure 7. For high amplitude waves, this linear analysis is not reliable. Experimentally, it seems that there is indeed little propagation, but that damping is rather slow. There is some disadvantage in not getting the waves to the outer boundary, where a non-reflecting boundary condition could have helped to expel them. Figures 8 and 9 demonstrate this. Later, our two-dimensional experiments will confirm that l should not in fact be taken too large.

4 Generalization to Two Space Dimensions

4.1 Modification of the 2D Euler Equations

The modified momentum equations will now be:

$$\begin{aligned} (\rho u)_t + (p + \rho u^2)_x + (\rho uv)_y &= -la\rho_{xt}, \\ (\rho v)_t + (\rho uv)_x + (p + \rho v^2)_y &= -la\rho_{yt}. \end{aligned} \qquad (6)$$

The other equations will retain their original form.

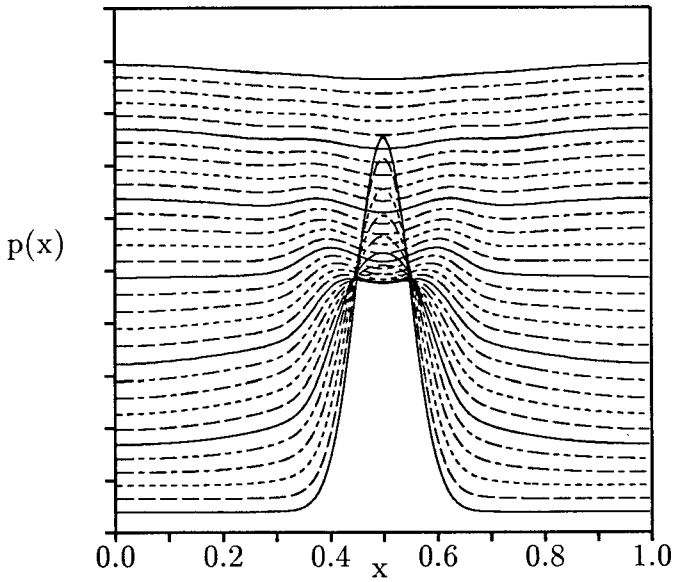

Figure 8: Nonlinear wave evolution by modified Euler equations, $\frac{l}{\Delta x} = 25$

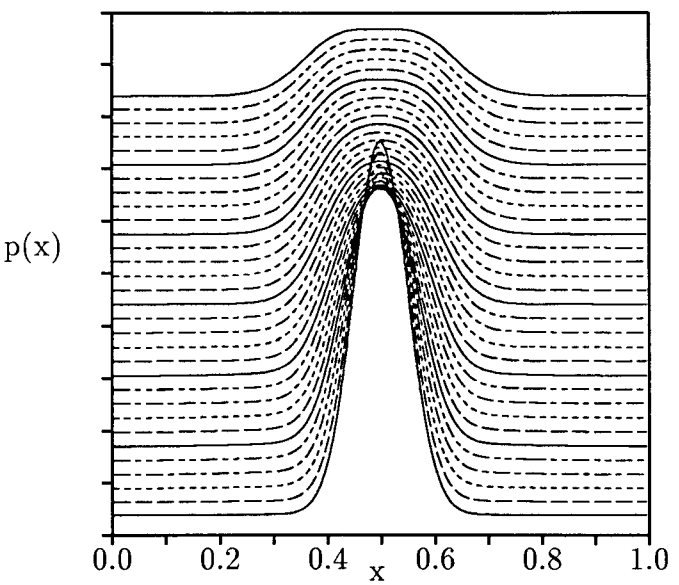

Figure 9: Nonlinear wave evolution by modified Euler equations, $\frac{l}{\Delta x} = 100$

4.2 Explicit Numerical Discretization

We integrate Equations 6 over one 2D numerical cell, and apply Green's Theorem to get

$$
\begin{aligned}
(\rho u)_{ij}^{n+1} &= (\rho u)_{ij}^{n} \\
&-\frac{\Delta t}{\mathcal{A}} \sum F_{2n}^{\star} \Delta S \;-\; \frac{\Delta t.l.a_o}{\mathcal{A}} \oint_{\text{cell faces}} (\rho_t) dy, \\
(\rho v)_{ij}^{n+1} &= (\rho v)_{ij}^{n} \\
&-\frac{\Delta t}{\mathcal{A}} \sum F_{3n}^{\star} \Delta S \;+\; \frac{\Delta t.l.a_o}{\mathcal{A}} \oint_{\text{cell faces}} (\rho_t) dx.
\end{aligned}
\tag{7}
$$

Here $F_{2n}^{\star}$ and $F_{3n}^{\star}$ are entries from the flux functions, calculated using upwind or central difference methods.

One inexpensive way to evaluate ρ_t on the cell faces (for the line integral) is to take an average of the adjacent cells, to get:

$$
\begin{aligned}
\oint_{\text{cell faces}} (\rho_t) dy = (\rho_t)_{i+1,j} \Delta y_{i+\frac{1}{2},j} + (\rho_t)_{i,j+1} \Delta y_{i,j+\frac{1}{2}} \\
+(\rho_t)_{i-1,j} \Delta y_{i-\frac{1}{2},j} + (\rho_t)_{i,j-1} \Delta y_{i,j-\frac{1}{2}}.
\end{aligned}
\tag{8}
$$

and a similar equation will be found for y-momentum equation. To ensure stability, analogy with the one-dimensional case suggests that for explicit calculations, the value of l should be proportional to a local length scale, say, the average side length of the cell concerned.

4.3 Explicit Numerical Computations

Let's use the standard NACA0012 airfoil problem, for M=0.63 and two degrees angle of attack. As a stable platform to test our modifications, we used initially a first-order upwind scheme. The surface boundary condition is the usual solid wall condition. The outer boundary is applied using the far field vortex solution. For the boundary condition for the new term, residuals are assumed to be zero in the ghost cells.

In Figure 10 the residual history for the original (non-viscous) code (solid line), and the code involving artificial bulk viscosity (dotted line) are compared. The history of the lift coefficient, for the same two codes, shows that the addition of bulk viscosity weakens the strong traversing waves.

We ran experiments with much larger values of l, and for which smaller timesteps were needed. This was to see whether an implicit code would be worth developing. The convergence history was plotted against a "pseudo iteration number"

$$
N^{*} = N \times \frac{\text{'inviscid' timestep}}{\text{actual timestep}}
$$

If the convergence had continued to improve on this basis, there would have been hope that an implicit code would

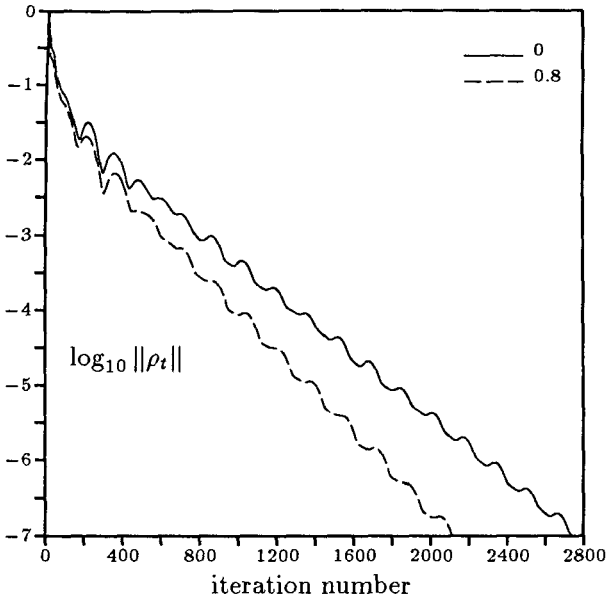

Figure 10: History of evolution of the residual $\frac{1}{N}\sum \log_{10} ||\rho_t||$. The dotted line shows the effect of adding bulk viscosity with $l = 0.8\Delta x$ to a 1st-order upwind code.

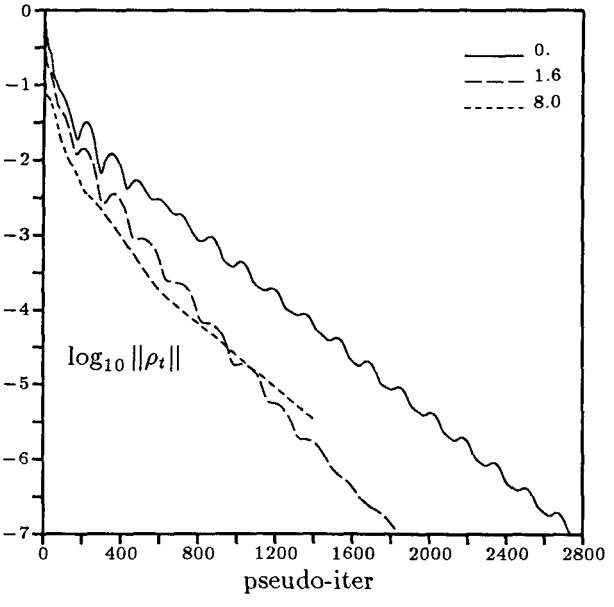

Figure 11: History of evolution of the residual $\frac{1}{N}\sum \log_{10} ||\rho_t||$. showing the use of larger BVD coefficients.

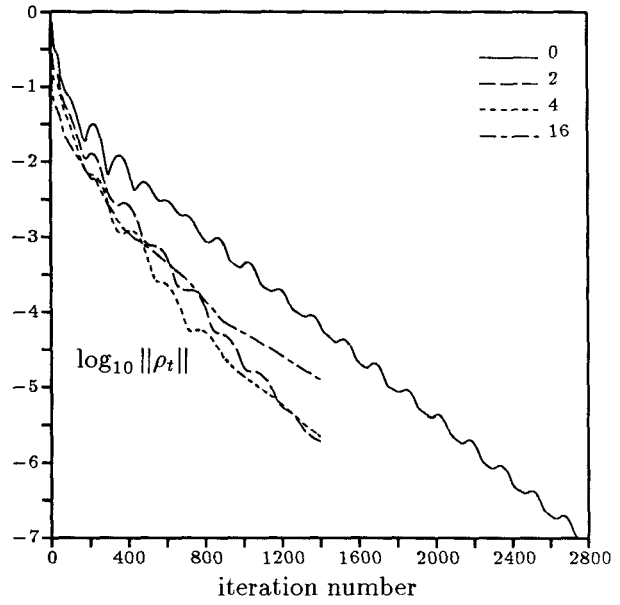

Figure 12: Evolution of the residual for different values of BVD coefficient obtained by an implicit method

have produced a similar history. In fact, Figure 11 shows that increasing the bulk viscosity is not always helpful. As in one dimension, it seems that large values of bulk viscosity slow down the movement of the waves through the flow field, so that a basic mechanism of wave removal across the outer boundary is lost.

Video movies showing the spatial distribution of the residuals show that using large values of l does damp out the waves during the early stages, but that a static pattern then develops that is very slow to disappear.

4.4 Implicit Numerical Discretization

To make higher values of bulk viscosity coefficients possible, an implicit formulation of the momentum equations is necessary. Such a method was implemented, despite the somewhat pessimistic conclusions reached above. Details can be found in [4]. The most direct approach led to a block-pentadiagonal system of equations, and failed to preserve exactly the original steady solution. A second attempt, using an ADI strategy, did preserve the original solution, and required only the solution of block-tridigonal systems. Nevertheless, the best we could do still imposed about a 25% overhead on the running time.

Figure 12 shows typical results. It can be seen that the gains barely outweigh the 25% penalty.

5 Comparison with Other Techniques

5.1 Residual Smoothing (RS)

The maximum permissible time step for explicit calculation of Euler equations (before addition of BVD terms) is restricted by the stability limit on the Courant number. It was observed by Jameson [5] that this restriction can be relaxed by replacing the residual at each point by a weighted average of the neighboring residuals. Consider a system of equations in one space dimension:

$$\mathbf{u}_t + \mathbf{f}_x = 0, \qquad \mathbf{R}(\mathbf{u}) = -\mathbf{f}_x,$$

where $\mathbf{u}, \mathbf{f} \in I\!R^n$, and $\mathbf{R}(\mathbf{u})$ is the vector of residuals. Residual soothing consists of replacing R by a smoothed value $\overline{\mathbf{R}}$, defined either explicitly by

$$\bar{\mathbf{R}} = (1 + \epsilon_x \delta_x^2)\mathbf{R}, \tag{9}$$

or implicitly by

$$(1 - \epsilon_x \delta_x^2)\bar{\mathbf{R}} = \mathbf{R}. \tag{10}$$

where δ_x is the central difference operator in the x direction, and ϵ_x is the corresponding smoothing parameter. In two space dimension, one may just add another term $(\epsilon_y \delta_y^2)$ inside the parantheses. In practice the best convergence rate may be found [5] by using time-steps about three times larger than the Courant number of the non-smoothed scheme suggests, and taking the smoothing parameter as large as possible while maintaining stability.

Performing this smoothing at the differential equation level for the one-dimensional acoustic equations gives

$$\begin{aligned} \rho_t + \rho_0 u_x &= \epsilon \rho_{txx}, \\ u_t + \frac{1}{\rho_0} p_x &= \epsilon u_{txx}, \\ p_t + \rho_0 a_0^2 u_x &= \epsilon p_{txx}. \end{aligned} \tag{11}$$

This changes the dispersion relationship to give

$$\frac{\omega_r}{\xi a_0} = \frac{\pm 1}{\sqrt{1 + \epsilon \xi^2}}, \tag{12}$$

with $\omega_i = 0$. This shows that residual smoothing works by increasing the propagation speed, and does not, at the differential equation level, introduce damping at all. It can also be seen that it is chiefly effective at high frequencies.

Since BVD does introduce damping, even at relatively low frequencies, it is be expected that the two techniques will be complementary.

5.2 Soft Wall Boundary Conditions (SWBC)

In refs [1,4] the idea was proposed of replacing the standard solid wall boundary conditions by something that allowed incoming waves to be reflected with reduced amplitudes, over an extended time. Such a condition can be written as

$$u_t + \frac{u}{\tau} = \frac{\mu}{\rho a} p_t, \tag{13}$$

where τ, μ are parameters to be chosen from within certain not very critical ranges. In this work we have used $\mu = 0.5$ and $\tau = 50\Delta t$. The numerical implementation is explained in [1,4], where gains of up to 40% were found for subcritical flows.

Since this mechanism operates quite independently from the others, we may hope to find that a combination of all three is particularly effective.

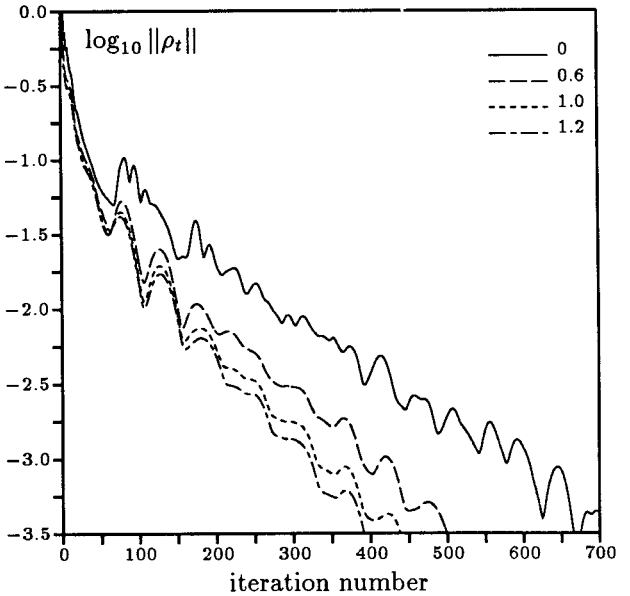

Figure 13: Comparison of residual history for different values of BVD in a central-differencing code

6 Modifying a Central-Differencing Code

For the details of the central differencing code used here see [5]. We will use the same standard NACA0012 airfoil problem as previously. Figure 13 compares the residual history for different values of bulk viscosity coefficient, added explicitly. It was found experimentally that the code is stable for values of l up to $1.3\Delta x$.

The speedup due to BVD appears to be rather greater in this case than in our first experiments with the upwind code. Presumably this is because we are dealing here with a second-order code, the regular form of which has less natural dissipation. The lift coefficient also converges very smoothly and very fast to the correct steady state solution.

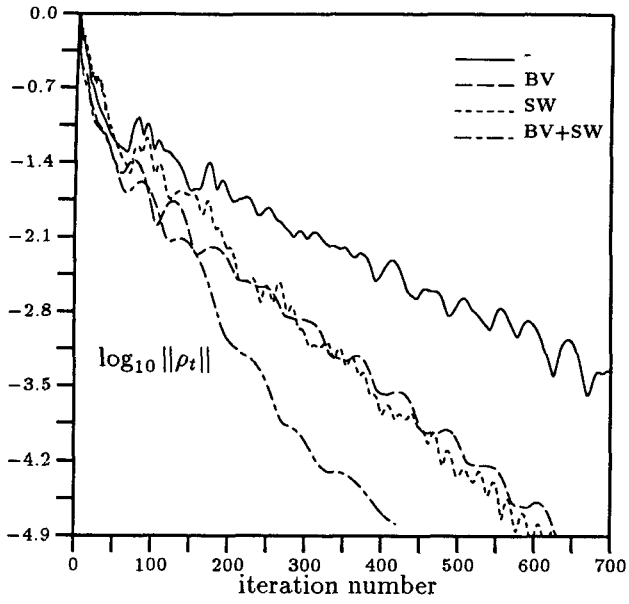

Figure 14: Combination of the SWBC and BVD in the central-differencing code, $M = 0.63$, without RS

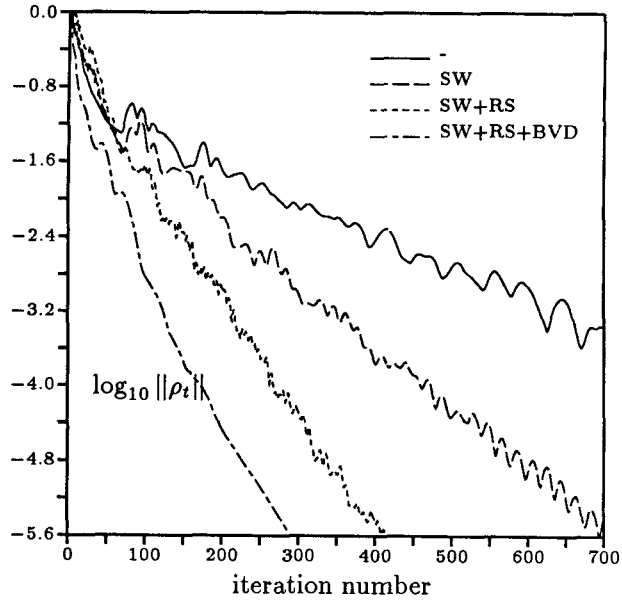

Figure 15: Effect of combining all three acceleration techniques on the residual history of the central-differencing code, $M = 0.63$, with RS $\nu = 2.$, $\epsilon = 0.2$, and BVD ($l = 1.3\Delta S$)

6.1 Combination of BVD and SWBC

Figure 14 shows the effect of combining BVD with the soft-wall BC. As compared with the basic method, either modification by itself cuts the iterations to about 60% of the number originally required. In combination, the gains are multiplied, and only about 36% of the original iterations are needed. We repeat that both modifications add negligable overhead to the time per iteration.

6.2 Combination of BVD, SWBC, and RS

To implement RS in two dimensions, using *approximate factorization*, we will write the 2D modified form of Equation 10 as

$$(1 - \epsilon\delta_x^2)(1 - \epsilon\delta_y^2)\bar{R}_{ij} = R_{ij},$$

and then we will solve consecutively two tri-diagonal systems, generated from equations

$$(1 - \epsilon\delta_x^2)Q_{ij} = R_{ij}^{n+1},$$

$$(1 - \epsilon\delta_y^2)\bar{R}_{ij}^{n+1} = Q_{ij},$$

with appropriate boundary conditions.

Figure 15 shows the effect of combining all three acceleration methods. Now, only about 20% of the original iterations are required, and the overhead remains less than 5%.

7 Low and High Mach Numbers

7.1 Low Mach Number

Central-differencing codes have generally been found to converge rather slowly at low Mach numbers. We discovered that adding a little BVD in explicit form not only made the process very smooth and well-behaved, but also increased the convergence rate very significantly. Figure 16 shows the residual history for the same airfoil problem, at a Mach number of 0.3. The number of iterations in this case is reduced to about 25% by BVD alone. It is interesting that the convergence plot is also far less 'noisy'.

The regular code was unable to produce a converged solution for M=0.01. The residual was reduced by about two orders of magnitude after 250 iterations, but then started to diverge. After adding BVD, smooth convergence was achieved at the same rate as in Figure 16.

7.2 High Mach Number

Unfortunately, the bulk viscosity method turns out to be rather ineffective in transonic flow. Figure 17 shows the effect of adding small amounts of BVD to the NACA 0012 test case at M=0.85, with $\alpha = 2^o$. In the best case the improvement is only just detectable, and in the worst case convergence is stalled.

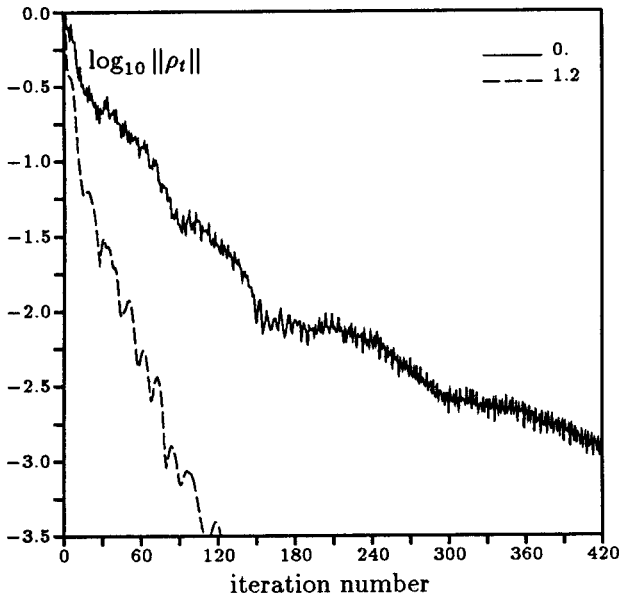

Figure 16: Effect of BVD combined with RS on the residual history RS in low Mach number flow, $M = 0.3$

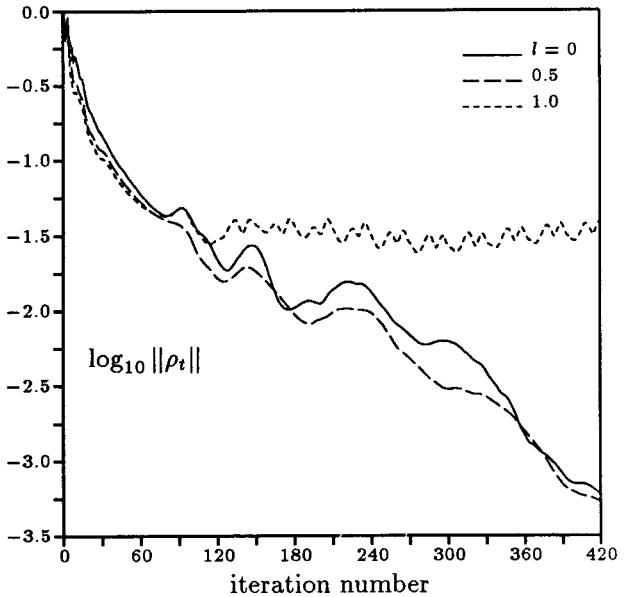

Figure 17: Effect of BVD on residual history in the CD code for a transonic case, $M = 0.85$, $\alpha = 2^o$

We believe that this can be explained in terms of the insights into convergence gained from the experiments reported in [1] and [4]. The mechanism of convergence seems to be greatly altered by the presence of embedded shocks. On the one hand, these often absorb the wandering acoustic waves themselves, leaving little for BVD to accomplish. However, the shocks may be very slow to find their own final equilibrium positions, and this is usually the determining factor as regards transonic convergence. It seems to us that quite a different acceleration device will be required in this case.

8 Conclusions

Bulk Viscosity Damping has been introduced, analyzed, and applied to the Euler equations in one and two space dimensions. It was shown that BVD can be added as an simple module to most current codes, written for subsonic compressible flows, and with no significant extra computation, the rate of convergence can be increased significantly. The best value for the characteristic length required seems to be close to the local mesh size. With this choice the timestep of the regular inviscid code can be retained, or even increased if residual smoothing is employed. Larger values require elaborate implicit methods that do not pay off.

With a simple explicit scheme, we have found gains of between 40 and 80%; the gains are most pronounced at low Mach numbers. The method complements very well other techniques for convergence acceleration. We have found that combining it with residual smoothing and a soft wall boundary condition is particularly effective, and carries an extremely low overhead.

References

1. K.Mazaheri and P.L.Roe, New light on numerical boundary conditions, in *AIAA 10th Computational Fluid Dynamics Conference*, AIAA CP 914, 1991.

2. J.D.Ramshaw and V.A.Mousseau, Accelerated artificial compressibility method for steady-state incompressible flow calculations, *Computers and Fluids*, vol. 18, p. 361, 1990.

3. A.J. Chorin, A numerical method for solving incompressible flow problems, *J. Comput. Physics*, vol. 2, p. 12. 1967.

4. K. Mazaheri, Numerical Wave Propagation and Steady State Solutions, Ph. D. Thesis, University of Michigan, 1992.

5. A. Jameson, Numerical solution of the Euler equations for compressible inviscid fluids, in *Numerical Methods for the Euler equations of Fluid Dynamics*, eds. F.Angrand et.al.. SIAM 1985.